

# R<sup>3</sup>: Reconstruction, Raw, and Rain: Deraining Directly in the Bayer Domain

Nate Rothschild  
Department of ECE  
Technion, Israel

nate.emails.i@gmail.com

Moshe Kimhi  
Department of CS  
Technion, Israel

moshekimhi@cs.technion.ac.il

Avi Mendelson  
Department of CS  
Technion, Israel

mendlson@technion.ac.il

Chaim Baskin  
School of ECE  
Ben-Gurion University  
chaimbaskin@bgu.ac.il

## Abstract

*Image reconstruction from corrupted images is crucial across many domains. Most reconstruction networks are trained on post-ISP sRGB images, even though the image-signal-processing pipeline irreversibly mixes colors, clips dynamic range and blurs fine detail. This paper uses the rain degradation problem as a "use case" to show that these losses are avoidable and show that learning **directly on raw Bayer mosaics** yields superior reconstructions. To substantiate the claim we (i) evaluate post-ISP and Bayer reconstruction pipelines, (ii) curate RAW-RAIN, the first public benchmark of real rainy scenes captured in both 12-bit Bayer and bit-depth-matched sRGB, and (iii) introduce **Information Conservation Score (ICS)**, a color-invariant metric that aligns more closely with human opinion than PSNR or SSIM. On the test split our raw-domain model improves sRGB results by up to **+0.99 dB PSNR** and **+1.2 % ICS**, while running faster with lower GFLOPs. The results advocate an ISP-last paradigm for low-level vision and open the door to end-to-end learnable camera pipelines.*

## 1. Introduction

Image corruption reconstruction is a well studied field, has very real world applications; automotive, security systems, and photography. Rain distorts image information, degrading both visual aesthetics as well as compute information extraction (i.e tracking, detection, segmentation, etc.). We use deraining as a use case example to display the benefits of reconstruction prior to the image signal processor. The ISP pipeline is designed to produce visually pleasing images for human consumption. However, from a restoration standpoint, it is a lossy and irreversible transformation.

Demosaicing introduces interpolation artifacts and blends spatially localized features. White balancing and color correction alter pixel intensities based on learned or estimated illumination models, often distorting the true spectral distribution. Furthermore, tone mapping and compression reduce dynamic range and quantize fine-grained intensity differences. These processes collectively destroy or obscure the low-level features and high-frequency details that are often essential for distinguishing corruption from image content. Consequently, reconstruction in the sRGB (we use sRGB and RGB interchangeably, all work in the paper is done in the sRGB space) domain becomes an ill-posed problem, requiring the model to not only detect and remove corrupting artifacts, but also to disentangle the impact of ISP transformations that are often scene- and device-dependent.

In this paper, we demonstrate the advantage of reconstruction done in the Bayer domain, significantly preserving information and fidelity. Samples of Bayer domain reconstruction and sRGB reconstruction can be viewed in Fig 1. Bayer images represent the closest approximation to the original sensor measurement, preserving spatial and photometric information. Each pixel corresponds to a direct photo-detection measurement with minimal transformation, offering a linear response to scene illumination and full access to high-frequency information before it is smoothed or distorted by the ISP. Our contributions are:

1. We demonstrate the significance of reconstruction in the Bayer domain over the post ISP domain.
2. We introduce a new Color-Invariant metric for image fidelity, correlated with human preference.
3. We introduce a novel dataset comprising temporally synchronized dual-camera video sequences captured in both Bayer (raw) and sRGB (post-ISP) formats.
4. We advocate for a shift in low-level vision tasks toward pre-ISP processing, and demonstrate its benefits in the



Figure 1. Columns Left-to-Right: Original (GT) image, Corrupted (rain) image, Bayer pipeline reconstruction, sRGB pipeline reconstruction

context of image deraining along with the added benefit of lower power consumption.

## 2. Related Work

### 2.1. Raw/Bayer-Domain Image Processing

Processing directly in the raw Bayer domain has emerged as a promising alternative to sRGB-based pipelines for tasks where high-fidelity signal recovery is critical. Several studies have demonstrated the advantages of operating on raw sensor data for denoising, reconstruction, and detection.

Liu *et al.* [12] introduced a learning-based denoising pipeline that operates directly on raw Bayer data, proposing Bayer pattern unification and Bayer-aware data augmentation to ensure robustness across different camera sensors. Their work showed that denoising in the raw domain results in significantly better fidelity than RGB-based denoising. Zhou *et al.* [28] proposed raw Bayer pattern synthesis using generative models to enable end-to-end vision system design from raw data, bypassing ISP entirely. Their results indicate that models trained on synthetic Bayer images can rival those trained on real sRGB images in downstream tasks like detection.

In feature-level processing, Zhou *et al.* [27] showed that extracting gradients directly from Bayer images preserves critical edge information that is often blurred by demosaicing, leading to more robust descriptors for matching and recognition. In the context of high dynamic range (HDR) imaging, Bayer-domain methods have also proven beneficial. For example, Kang *et al.* [4] demonstrated that fusing exposures before ISP yields better HDR reconstructions due to the linear radiometric space of raw images. Schwartz *et al.* [16] demonstrates object classification and semantic segmentation in the RAW domain outperform the RGB domain. Schwartz *et al.* [15] goes a step further and replaces the ISP, mapping the RAW domain directly to the sRGB domain, by use of a neural network.

Despite these advantages, little attention has been given to applying such raw-domain processing techniques to image deraining. To the best of our knowledge, our work is the first to explore deraining directly on Bayer images as a show case for image reconstruction. Our method enables more accurate modeling of rain streaks and significantly improves reconstruction quality. While there has been work done, regarding reconstruction in the Bayer domain, the work is done mostly in denoising, a statistically well modeled form of corruption. In contrast, rain streaks exhibit high-frequency, directional patterns and often introduce spatial occlusions and intensity shifts that interact non-trivially with the color filter array.

### 2.2. Single-Image Deraining

Single-image deraining is a well-studied problem, where the objective is to recover a clean image from one degraded by rain streaks. Early approaches relied on hand-crafted priors such as sparsity and low-rank assumptions

to separate rain from background content. More recently, deep learning-based methods have become the dominant paradigm. These include RainNet [22], DID-MDN [24], and RESCAN [11], which leverage convolutional neural networks (CNNs) to model the complex spatial patterns of rain. Attention-based methods, such as RCDNet [18], further improve performance by emphasizing relevant spatial and channel features. However, nearly all these methods operate on post-ISP sRGB images.

Some recent works Hu *et al.* [3] attempt to address domain-specific generalization using synthetic rain or Yasarla *et al.* [23] sensor-aware data augmentation, but they still operate within the sRGB domain, where sensor-level fidelity is lost.

### 2.3. Multi-view and Stereo Deraining & Reconstruction

Early geometry-based studies already hinted that **a second viewpoint can help suppress rain artifacts**. Kim *et al.* [5] went further and combined temporally adjacent frames with the opposite stereo view to inpaint rain-covered regions. Although effective, classical methods depend on heuristic matching and struggle with fine-scale streaks or heavy rain.

With deep learning, **stereo-aware deraining networks** have emerged. Zhang *et al.* proposed PRRNet/EPRRNet [25], which fuse semantic priors with binocular cues to refine rain removal. Wei *et al.* introduced StereoIRR [19], employing Dual-View Mutual Attention to enhance cross-view feature interaction, while Wen *et al.* developed MQINet [20], a query–interaction transformer that attains state-of-the-art stereo deraining accuracy. All these methods operate on **post-ISP sRGB images**; none exploit raw Bayer data, so they inherit the ISP’s nonlinear distortions discussed in Section 2.2.

Stereo cues have likewise benefited other **low-level reconstruction tasks**. DAVANet [26] aggregates depth-aware features for stereo deblurring; DiffStereo [1] introduces high-frequency-aware diffusion modelling for stereo super-resolution, deblurring and low-light enhancement. Dual-camera pipelines have also been explored for burst denoising–deblurring [17], further illustrating the complementary nature of synchronized viewpoints.

To the best of our knowledge, no published work unifies rain removal *before* any ISP step, nor evaluates such a model on **real** Bayer images paired with matched sRGB images. By learning directly on raw mosaics, releasing the first raw-rain benchmark, and introducing the color-invariant ICS metric, our study bridges the gap between sensor-level processing and deraining, establishing a new baseline for *ISP-last* low-level vision.

## 3. Methodology

Our deraining framework is designed to investigate the impact of performing deraining in the raw sensor space against the sRGB space. To facilitate this comparison, we process dual-camera stereo image pairs using a custom software-based ISP pipeline and a dedicated neural network architecture for rain removal.

### 3.1. Software ISP Pipeline

To convert raw Bayer images into sRGB images for the sRGB-space experiments, we developed a software ISP pipeline that simulates key operations typically performed in camera hardware. This pipeline includes the following sequential stages: black level subtraction, demosaicing, lens shading, white balancing, color correction, global tone mapping, local tone mapping, and gamma. Each stage closely follows established methods to mimic realistic ISP behavior, enabling a fair comparison between raw and post-ISP representations.

Figure 2 illustrates the complete software ISP pipeline. The pipeline ensures that Bayer/sRGB images fed into the deraining network preserve photometric properties comparable to standard camera outputs.

### 3.2. Deraining Model Architecture

Our goal is *not* to invent a new heavy-weight network but to show that **even a very small, textbook U-Net** benefits from operating on raw Bayer data. Therefore we propose three architectures that follow the simplest design and still deliver competitive performance. The three architectures follow the same rough design as follows:

- **Input stem.** A single  $3 \times 3$  convolution maps the image to  $C = 32$  features. We instantiate *two* stems that differ only in the number of channels:  $3 \rightarrow 32$  for RGB and  $1 \rightarrow 32$  for the Bayer tensor. Apart from this first layer, *all remaining layers are identical* across the two training regimes.
- **Backbone.** A four-level encoder–decoder U-Net with stride-2 convolutions for down-sampling and bilinear up-sampling in the decoder. Each level contains two ConvBN-ReLU blocks; no dilations or large kernels are used.
- **Attention.** For the CBAM model, a lightweight Convolutional Block Attention Module (CBAM) [21] is inserted at (i) the bottleneck and (ii) after each decoder up-convolution. CBAM adds just 0.06 M parameters ( $< 4\%$  of the total) yet sharpens rain-streak localisation.
- **Output head.** A final  $3 \times 3$  convolution restores the original channel count (3 for RGB, 1 for Bayer) followed by a residual “rain mask” summation:  $\hat{I} = \alpha_1 X + \alpha_2 \Delta$ .

Input to the models are original images, sRGB (B,3,H,W) or Bayer (B,1,H,W). The model outputs the input image reconstructed (derained) of same dimensions.

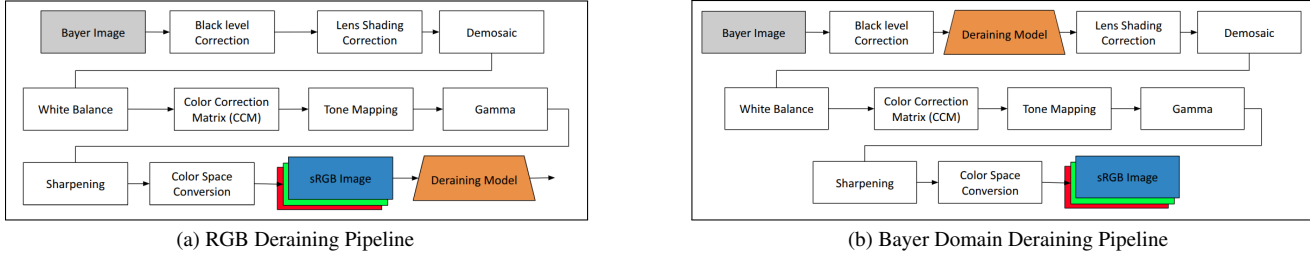


Figure 2. Identical Pipeline Architectures, only deraining model location varies

The the model calculates  $\alpha_1$  &  $\alpha_2$  for each pixel in each frame, this is to provide model stability and input information retention throughout the model.

The three models are the UNET, MONOCULAR UNET, and CBAM. The UNET and MONOCULAR UNET differ by use of stereo input vs single sensor input. The UNET and CBAM differ by lowest level of the Unet being standard convs vs. CBAM blocks.

### 3.3. Color-Invariant Reconstruction Metric

Conventional full-reference metrics—**PSNR**, **SSIM**, and **LPIPS**—assume that the reference and the reconstruction live in *exactly the same radiometric space*. This assumption collapses in deraining because heavy rain corrupts the statistics that drive the camera *image-signal-processing* (ISP) stack. A single streak can bias the auto-white-balance; dense drizzle alters the color-correction matrix; veiling glare fools the tone-mapper. Figure 3 clearly demonstrates this, the ground truth image generates white balance/color correction different from the corrupt (rain) image. When the reconstruction is applied, heavily affects the white balance. When done prior the ISP (Bayer reconstruction) we get a white balance similar to the ground truth, while post-ISP correction retains the corrupted images white balance. Consequently, even if a method perfectly restores the raw Bayer measurements, running the restored image through the ISP will yield a *sRGB frame that is systematically shifted*—in brightness, color temperature and local contrast—relative to an ISP pass computed from the clean ground truth. Standard metrics then penalize the algorithm for differences introduced *after* reconstruction:

- **PSNR** measures mean-squared error per pixel; any global gain change, gamma offset or sub-pixel mis-registration produces large penalties. While over-smoothing (loss of detail) can often achieve high PSNR
- **SSIM** compares luminance, contrast and phase locally, yet remains blind to frequency-domain losses (fine rain-induced blur) and is still upset by unavoidable tone-mapping differences.
- **LPIPS** embeds images with a network trained on Internet sRGB photos; its channels are color-sensitive and brittle to gamut shifts caused by per-image ISPs.

Hence these scores *confound ISP variance with restoration quality*, rewarding color mimicry over information preservation. For deraining—and any restoration that precedes a nonlinear, scene-dependent ISP—we require a metric that discounts benign color-space shifts while remaining sensitive to structural and spectral fidelity. We therefore introduce the *Information Conservation Score (ICS)*, which couples a color-agnostic multi-scale SSIM term with a frequency-matching KL-divergence. ICS correlates far better with human preference when the input undergoes strong distortions or is evaluated across heterogeneous ISP pipelines. We conducted thorough human trials, with a double blind experiment. Displaying three images, the ground truth, a Bayer pipeline reconstructed image, and a RGB pipeline reconstructed image. The subject was tasked with selecting a reconstructed image that appeared closer to the ground truth. We found the highest correlation with the ICS metric details under Table 1

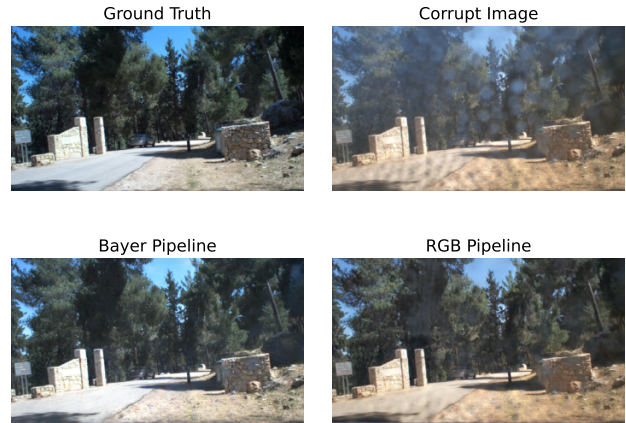


Figure 3. Clockwise, Top-Left; **Ground Truth, Rainy** - raindrops skew WB/CCM statistics, **RGB Pipeline** - rain removal done after WB/CCM statistics, color similar to rainy image, **Bayer Pipeline** - Rain removal prior ISP, WB/CCM statistics similar to GT

PSNR, being a pixel-wise measure based on mean squared error, is highly sensitive to minor spatial misalignments, brightness shifts, or perceptual variations, and thus

Table 1. Human trial results, 12 subjects conducted a “Two-alternative forced choice (2AFC) pairwise comparison test with reference” of between 50-200 images reconstructed selection. First two columns are subjects image selection, the columns are mutually exclusive. Last 3 columns display the number of times the image with the higher metric was selected, for some images more than one metric was higher for the selected image, explaining the overlap.

Subject	Bayer	RGB	ICS	SSIM	PSNR
Avg.	76.4%	23.6%	<b>77.2%</b>	73.4%	71.7%

fails to capture semantic or structural fidelity. SSIM partially addresses this by comparing local patterns of luminance, contrast, and structure, but remains confined to the spatial domain and is largely blind to degradations in the image’s spectral composition—particularly the loss of high-frequency components like fine textures and edges. LPIPS, while perceptually motivated, relies on deep features that were trained on sRGB images, making it similarly biased toward color consistency.

For our task, the primary objective is to evaluate how well structural information—such as edges, contours, and fine details—is preserved through the deraining process, irrespective of whether the output appears color-accurate, similar to recent studies about the frequencies decomposition of images for deep learning [10].

To this end, we propose the *Information Conservation Score (ICS)*, which more faithfully quantifies the preservation of signal content by integrating both spatial and frequency domain analyses. ICS combines a spatial-domain term based on *multi-scale SSIM (MS-SSIM)*, which captures perceptual structural similarity, with a frequency-domain term based on the *Kullback–Leibler (KL) divergence* between the normalized power spectra of the original and reconstructed images. This dual-domain formulation enables ICS to penalize not only spatial inconsistencies but also frequency-domain distortions and spectral energy loss—factors often overlooked by SSIM and entirely invisible to PSNR.

Additionally, ICS is designed to be *color-invariant* and *phase-tolerant*, making it better suited for applications where exact color fidelity or pixel-wise alignment is less relevant. Such scenarios include raw sensor processing, inverse problems in computational photography, and learned image-to-image translation tasks, where outputs may exhibit minor color or phase variations while still preserving essential scene content. In these cases, SSIM and PSNR may assign unfairly low scores to reconstructions that are perceptually and structurally sound. ICS, by contrast, provides a more meaningful and discriminative assessment of informational integrity.

Therefore, ICS offers a more comprehensive and interpretable metric for evaluating image reconstruction quality, particularly in settings where the preservation of *information*, rather than strict pixel-level fidelity, is the primary ob-

jective.

The proposed **Information Conservation Score (ICS)** Eq. 1 combines perceptual similarity with frequency-domain fidelity:

$$\text{ICS}(X, \hat{X}) = \lambda \cdot \text{MS-SSIM}(X, \hat{X}) + (1 - \lambda) \cdot D_{\text{KL}} \left( \tilde{P}_X(u, v, w) \parallel \tilde{P}_{\hat{X}}(u, v, w) \right) \quad (1)$$

$$\tilde{P}_X(u, v, w) = \frac{|\mathcal{F}\{I(x, y, x)\}(u, v, w)|^2}{\sum_{u, v, w} |\mathcal{F}\{I(x, y, x)\}(u, v, w)|^2} \quad (2)$$

- **MS-SSIM:** Multi-scale SSIM captures structure at various spatial resolutions.
- $\tilde{P}_X(u, v, w)$ : Normalized 3D (2D for gray scale) power spectrum of image  $X$  over frequency coordinates  $(u, v, w)$ .
- $D_{\text{KL}}$ : Kullback–Leibler divergence between spectral distributions.
- $\lambda$ : Balancing coefficient.

Rain streaks are *anisotropic, high-frequency* structures. Any derainer that aggressively smooths the image will score well in pixel-wise metrics yet visibly blur textures and edges. To guard against such “cheating” we compare the *normalized power spectra*  $\tilde{P}_X$  and  $\tilde{P}_{\hat{X}}$ . This choice has three key advantages:

1. **Color and phase invariance.** The magnitude of the Fourier transform ignores channel gains, hue shifts and sub-pixel phase offsets introduced by different ISPs, letting the metric focus on structural fidelity.
2. **High-frequency sensitivity.** Natural images exhibit a  $1/f^\alpha$  spectral decay, whereas rain removal often reduces energy at large  $(u, v, w)$ . The KL divergence acts like a “histogram distance” between the two spectra, heavily penalizing frequency bands whose energy has been suppressed—precisely the symptom of over-smoothing.
3. **Scale independence.** Because we normalize each spectrum to a probability mass function, the comparison is insensitive to global exposure or gain changes; it measures *shape* rather than absolute magnitude, complementing MS-SSIM’s luminance/contrast terms.

**Spectral KL as an information–loss proxy.** Let  $\mathcal{F}\{I\}$  denote the 2-D discrete Fourier transform and recall Parseval’s theorem, which equates spatial and frequency–domain  $\ell_2$  energy:

$$\sum_{x,y} I(x,y)^2 = \sum_{u,v} |\mathcal{F}\{I\}(u,v)|^2 = E_I.$$

Dividing every coefficient by the total energy converts the power spectrum into a probability mass function<sup>1</sup>  $p_I(u,v) = \tilde{P}_I(u,v)$ . When a derainer produces  $\hat{I}$ , the question becomes: *how much of the original spectral distribution is retained?*

**KL divergence bounds potential information loss.** Relative entropy  $D_{\text{KL}}(p_I|p_{\hat{I}}) = \sum_{u,v} p_I \log \frac{p_I}{p_{\hat{I}}}$  measures the coding overhead incurred when one represents coefficients drawn from  $p_I$  with a code optimized for  $p_{\hat{I}}$  Cover and Thomas [2]. By Gibbs’ inequality it is non-negative and zero *iff*  $p_I = p_{\hat{I}}$ . If high-frequency energy is suppressed (typical over-smoothing), mass is shifted from the “tail” of  $p_I$  to its low-frequency bins, inflating  $D_{\text{KL}}$  multiplicatively with the logarithmic term:

$$p_{\hat{I}}(u_h, v_h) \ll p_I(u_h, v_h) \implies p_I \log \frac{p_I}{p_{\hat{I}}} \uparrow.$$

Thus the KL term provides a *soft lower bound* on spectral information lost, complementing the phase-aware MS-SSIM factor.

**Connection to MSE.** Expanding the Taylor series of  $D_{\text{KL}}$  around  $p_I = p_{\hat{I}}$  gives, to second order,  $D_{\text{KL}} \approx \frac{1}{2} \sum_{u,v} \frac{(p_{\hat{I}} - p_I)^2}{p_I}$ , an  $\ell_2$  distortion that is *weighted inversely* by the original energy. Hence deviations in sparsely populated, typically high-frequency bins are penalized **more** strongly than the same absolute error in low frequencies—precisely the behavior we desire to discourage blur while remaining agnostic to color shifts.

In summary, the spectral KL component of ICS acts as an information–theoretic safeguard against over-smoothing, quantifying the expected penalty for discarding frequency content that is critical for sharp, rain-free reconstruction. We empirically show in Section 4 that this metric better reflects perceptual and structural fidelity when models are compared across raw and post-ISP domains.

### 3.4. Dataset Collection and Composition

To support our study on deraining in raw and sRGB spaces, we collected a custom stereo dataset using a dual-camera setup. The rig consists of two synchronized FLIR Blackfly S 2.8MP cameras, each capable of capturing raw Bayer images. All frames were recorded using a fixed analog gain

of 1 to maintain consistent signal amplification across varying conditions. Exposure times were varied between 300 ms and 10,000 ms to account for different lighting conditions throughout the day, including both bright daylight and low-light environments.

Data collection was carried out in a range of realistic scenarios. Some scenes were recorded through a stationary glass window, while others were captured from within a moving vehicle. To introduce a range of real-world rain artifacts, we included sessions with and without windshield wipers operating at different speeds. These variations enable evaluation of the model’s robustness to dynamic occlusions and motion-induced artifacts.

Popular rain datasets are computer synthetically generated. This rain dataset was collected by real world rain simulation. For this purpose, we used a rain system, which scatters water-rain-like droplets on the windshield and in depth of the scene. The ground truth images were collected prior to triggering the rain system, the rainy images collected immediately after with the rain system triggered. A rig was used to ensure spatial stability throughout the process.

Diversity of the data is paramount to achieving real world results, Figure 4 demonstrates how wide the data is across different measurements, mean value (lighting), variance values (dynamic range), and how diverse the corrupted data is compared to the ground truth by different metrics.

The dataset includes a total of 89 diverse training scenes, 30 identity training scenes, 10 held-out test scenes, 15 validation scenes (no GT). Each scene consists of temporally synchronized stereo image pairs in raw format. Each scene is a video sequence of 300 frames for each camera, for a total of **48,000 training frames, 18,000 identity frames, 6,000 test frames, 9,000 validation frames** which include driving scenes for evaluation.

Full RGB dataset

<https://huggingface.co/datasets/realrainmaker/RAW-RAIN-rgb>

Full Bayer dataset

<https://huggingface.co/datasets/realrainmaker/RAW-RAIN-bayer>

Train scene settings include 30 scenes behind glass window, 42 scenes within a vehicle, and 14 scenes in a vehicle with wipers.

Training data location varies, 17 forest location, 28 city location, 30 playground location, 11 parking lot location Validation set (used for visual testing only) includes, 5 driving scenes, 8 scenes with local motion, 2 static scenes.

Rain intensity is categorized as light, medium or heavy rain. The training set has 46 light rain, 29 medium rain, and 11 heavy rain scenes. Test set has 2 light rain, 6 medium rain, and 2 heavy rain scenes. A broad overlook of the data can be found in Table 2

<sup>1</sup>Because magnitudes are non-negative and sum to one, all axioms of a PMF are satisfied.

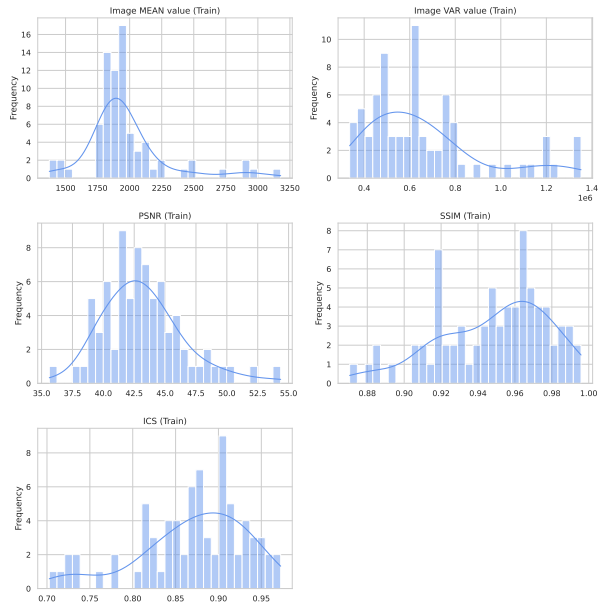


Figure 4. Diverse Training Data. Metrics calculated for rainy images compared with GT

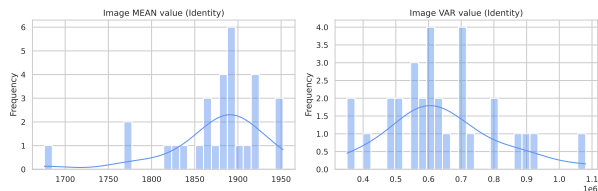


Figure 5. Identity Data real-world driving scenes, where input equal the gt. Allows for Synthetic data creation and training models for the identity operator

Table 2. RRS dataset statistics.

Split	Scenes	Frames	Rain dens.	Illum.
Train	86	48 000	light-heavy	day+evening
Identity	30	18 000	None	day
Val	15	9 000	light-heavy.	day+evening
Test	10	6 000	light-heavy	day+evening

## 4. Results

### 4.1. Experimental setting

**Raw-Rain-Stereo (RRS).** Table 2 summarises the proposed dataset. All frames are  $1080 \times 1920$  12-bit Bayer (RGGB). The ISP described in Sec. 3 converts them to 12-bit sRGB for RGB experiments (we omit quantization for fairer comparison). Aside from the architecture described in 3.2, we also compared results using simple UNET [14] in both stereo and mono scenarios across 10

complex scenes. For all experiments, we use AdamW, initial  $1 \times 10^{-4}$ , 600k iters, single batch, crops of  $512^2$ .  $\mathcal{L}_1$  Loss. Runtime  $\sim 8$  hours on RTX3090. We report PSNR, SSIM and the proposed ICS.

### 4.2. Quantitative Comparison

We conducted exhaustive testing on 10 scenes (300 frames each), using the balancing coefficient  $\lambda = \frac{1}{2}$ . Pitting the Bayer model against the RGB model. The results can be viewed in the following table 3. First thing to notice is the average across all scenes Bayer deraining outperforms sRGB deraining. Scene 3 is an anomaly, with regard to the standard metrics PSNR & SSIM, the models don't seem to have improved the images, this goes against visual inspection as shown in Fig 6. The ICS does capture the this improvement. Lastly across the test set, ICS consistently shows greater information conservation when deraining in the Bayer domain. Further investigation for the desired balancing coefficient is required.

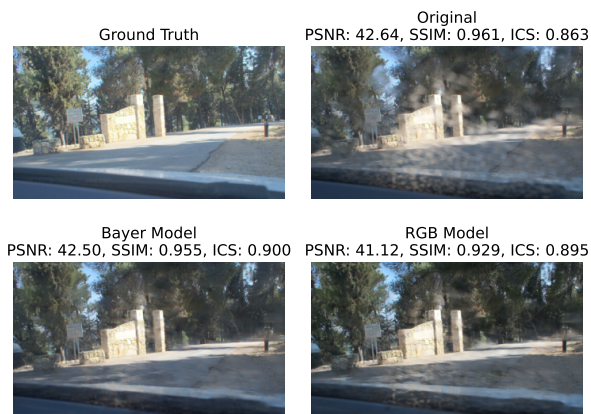


Figure 6. ICS reflects visual quality, where PSNR & SSIM fail. Visually reconstructed images (Bottom Images) are less corrupt, yet have lower PSNR\SSIM but higher ICS.

## 5. Conclusion

We showed that *sensor-level* deraining—learning directly on raw Bayer mosaics outperforms conventional post-ISP approaches. On the new RAW-RAIN benchmark our lightweight U-Net improves RGB baselines by up to **+0.99 dB PSNR** and **+1.2 % ICS**; as well as requires only a single-channel input, simplifying deployment on resource-constrained hardware.

We publish the first public set of paired 12-bit Bayer and bit-depth-matched sRGB rain scenes, enabling reproducible research on pre-ISP restoration; We created the **Information Conservation Score (ICS)**, a color-invariant metric that better aligns with human judgments than PSNR or SSIM.

Table 3. Bayer vs RGB improvement (test split) across 10 test scenes.

Model	Domain	Scene 1			Scene 2			Scene 3		
		PSNR	SSIM	ICS $\uparrow$	PSNR	SSIM	ICS $\uparrow$	PSNR	SSIM	ICS $\uparrow$
CBAM	Bayer	<b>46.742</b>	<b>0.965</b>	<b>0.945</b>	<b>51.781</b>	<b>0.993</b>	<b>0.964</b>	41.472	0.942	<b>0.864</b>
	RGB	44.87	0.957	0.925	47.867	0.986	0.948	40.257	0.917	0.852
UNET	Bayer	45.91	0.962	<b>0.939</b>	<b>52.084</b>	0.992	<b>0.963</b>	41.562	0.943	0.874
	RGB	<b>45.911</b>	<b>0.973</b>	0.937	50.663	0.992	0.96	41.01	0.934	<b>0.876</b>
MONO	Bayer	<b>47.053</b>	0.972	<b>0.948</b>	<b>51.973</b>	0.993	<b>0.965</b>	<b>41.945</b>	0.94	<b>0.879</b>
	RGB	46.03	0.972	0.944	51.311	0.993	0.961	41.146	0.937	0.877
Original		40.992	0.897	0.886	44.317	0.966	0.921	41.756	<b>0.954</b>	0.814
Model	Domain	Scene 4			Scene 5			Scene 6		
		PSNR	SSIM	ICS $\uparrow$	PSNR	SSIM	ICS $\uparrow$	PSNR	SSIM	ICS $\uparrow$
CBAM	Bayer	<b>47.538</b>	<b>0.985</b>	<b>0.905</b>	<b>42.848</b>	<b>0.961</b>	<b>0.807</b>	53.375	0.996	<b>0.966</b>
	RGB	45.939	0.976	0.879	41.854	0.953	0.791	<b>54.727</b>	0.996	0.965
UNET	Bayer	<b>47.769</b>	0.986	<b>0.912</b>	<b>43.915</b>	0.963	<b>0.814</b>	53.518	0.995	<b>0.969</b>
	RGB	46.108	0.986	0.909	42.756	0.963	0.812	<b>54.755</b>	0.995	0.968
MONO	Bayer	47.926	0.988	0.913	42.518	<b>0.964</b>	<b>0.814</b>	54.092	0.996	0.97
	RGB	<b>48.66</b>	0.988	0.913	<b>42.782</b>	0.963	0.812	<b>55.327</b>	0.996	0.97
Original		42.517	0.959	0.833	40.166	0.934	0.758	45.841	0.97	0.94
Model	Domain	Scene 7			Scene 8			Scene 9		
		PSNR	SSIM	ICS $\uparrow$	PSNR	SSIM	ICS $\uparrow$	PSNR	SSIM	ICS $\uparrow$
CBAM	Bayer	53.349	0.996	<b>0.97</b>	<b>51.144</b>	0.991	<b>0.955</b>	<b>42.823</b>	<b>0.96</b>	<b>0.9</b>
	RGB	<b>54.27</b>	0.996	0.966	50.571	0.991	0.95	40.999	0.949	0.884
UNET	Bayer	53.46	<b>0.995</b>	<b>0.972</b>	50.937	<b>0.993</b>	<b>0.958</b>	41.675	<b>0.964</b>	<b>0.899</b>
	RGB	<b>54.437</b>	0.992	0.969	<b>51.381</b>	0.992	0.956	<b>42.456</b>	0.961	0.893
MONO	Bayer	54.047	<b>0.996</b>	<b>0.972</b>	<b>51.624</b>	0.992	<b>0.958</b>	<b>44.793</b>	<b>0.968</b>	<b>0.907</b>
	RGB	<b>55.323</b>	0.993	0.97	51.45	0.992	0.957	43.363	0.967	0.903
Original		45.57	0.971	0.94	47.947	0.985	0.92	36.837	0.896	0.839
Model	Domain	Scene 10			Average					
		PSNR	SSIM	ICS $\uparrow$	PSNR	SSIM	ICS $\uparrow$			
CBAM	Bayer	<b>47.636</b>	0.984	<b>0.93</b>	<b>47.87</b>	<b>0.977</b>	<b>0.92</b>			
	RGB	47.491	0.984	0.924	46.884	0.97	0.908			
UNET	Bayer	47.214	0.985	0.924	<b>47.804</b>	0.977	<b>0.922</b>			
	RGB	<b>47.545</b>	0.985	0.924	47.702	0.977	0.92			
MONO	Bayer	47.214	<b>0.987</b>	<b>0.926</b>	<b>48.318</b>	<b>0.979</b>	<b>0.925</b>			
	RGB	47.682	0.985	0.925	48.307	0.978	0.923			
Original		45.957	0.977	0.905	43.19	0.95	0.875			

These findings advocate an **ISP-last** paradigm for low-level vision: preserve raw sensor data until the final stage, then apply a learnable or task-aware ISP. Future work includes joint training of ISP and restoration, extension to other degradations (fog, low-light, motion blur), and integration with burst or multi-modal inputs for further gains in

fidelity and efficiency [8, 9], as well as benefits for other domains such as noise in images [13] and labels [6, 7].

## References

- [1] Huiyun Cao, Yuan Shi, Bin Xia, Xiaoyu Jin, and Wenming Yang. Diffstereo: High-frequency aware diffusion model for stereo image restoration. *arXiv preprint arXiv:2501.10325*, 2025. 3
- [2] T.M. Cover and J.A. Thomas. *Elements of Information Theory*. Wiley, 2012. 6
- [3] Xiaowei Hu, Chi-Wing Fu, Lei Zhu, and Pheng-Ann Heng. Depth-aware single image rain removal via a two-stage network. In *CVPR*, 2019. 3
- [4] Hee Kang, Suk Ho Lee, Ki Sun Song, and Moon Gi Kang. Bayer-patterned hdr reconstruction using adaptive weighting function. *EURASIP Journal on Advances in Signal Processing*, 2014. 2
- [5] Jin-Hwan Kim, Jae-Young Sim, and Chang-Su Kim. Stereo video deraining and desnowing based on spatiotemporal frame warping. *IEEE International Conference on Image Processing, ICIP*, 2015. 3
- [6] Moshe Kimhi, Omer Kerem, Eden Grad, Ehud Rivlin, and Chaim Baskin. Noisy annotations in semantic segmentation. *arXiv preprint arXiv:2406.10891*, 2024. 8
- [7] Moshe Kimhi, Shai Kimhi, Evgenii Zheltonozhskii, Or Litany, and Chaim Baskin. Semi-supervised semantic segmentation via marginal contextual information, 2024. 8
- [8] Moshe Kimhi, Tal Rozen, Avi Mendelson, and Chaim Baskin. Amed: Automatic mixed-precision quantization for edge devices. *Mathematics*, 12(12), 2024. 8
- [9] Moshe Kimhi, Idan Kashani, Avi Mendelson, and Chaim Baskin. Hysteresis activation function for efficient inference, 2025. 8
- [10] Moshe Kimhi, Erez Koifman, Ehud Rivlin, Eli Schwartz, and Chaim Baskin. Waveclip: Wavelet tokenization for adaptive-resolution clip, 2025. 5
- [11] Xia Li, Jianlong Wu, Zhouchen Lin, Hong Liu, and Hongbin Zha. Recurrent squeeze-and-excitation context aggregation net for single image deraining. In *CVPR*, 2018. 3
- [12] Jiaming Liu, Chihao Wu, Yuzhi Wang, Qin Xu, Yuqian Zhou, Haibin Huang, Chuan Wang, Shaofan Cai, Yifan Ding, Haoqiang Fan, and Jue Wang. Learning raw image denoising with bayer pattern unification and bayer preserving augmentation. In *CVPR*, 2019. 2
- [13] Claudio Michaelis, Benjamin Mitzkus, Robert Geirhos, Evgenia Rusak, Oliver Bringmann, Alexander S. Ecker, Matthias Bethge, and Wieland Brendel. Benchmarking robustness in object detection: Autonomous driving when winter is coming, 2020. 8
- [14] Olaf Ronneberger, Philipp Fischer, and Thomas Brox. U-net: Convolutional networks for biomedical image segmentation, 2015. 7
- [15] Eli Schwartz, Raja Giryes, and Alex M. Bronstein. Deepisp: Toward learning an end-to-end image processing pipeline. *IEEE Transactions on Image Processing*, 28(2):912–923, 2019. 2
- [16] Eli Schwartz, Alex M. Bronstein, and Raja Giryes. Isp distillation. *IEEE Open Journal of Signal Processing*, 4:12–20, 2023. 2
- [17] Shayan Shekarforoush, Amanpreet Walia, Marcus Brubaker, and Alex Levinshtein. Dual-camera joint deblurring–denoising. In *CVPR*, 2024. 3
- [18] Tianyu Wang, Xin Yang, Ke Xu, Shaozhe Chen, Qiang Zhang, and Rynson W. H. Lau. Spatial attentive single-image deraining with a high quality real rain dataset. In *CVPR*, 2019. 3
- [19] Yanyan Wei, Zhao Zhang, Zhongqiu Zhao, Yang Zhao, Richang Hong, and Yi Yang. Stereo image rain removal via dual-view mutual attention. In *ECCV*, 2022. 3
- [20] Yuanbo Wen, Tao Gao, Ziqi Li, Jing Zhang, and Ting Chen. Multi-dimension queried and interacting network for stereo image deraining. In *ICCV*, 2023. 3
- [21] Sanghyun Woo, Jongchan Park, Joon-Young Lee, and In So Kweon. Cbam: Convolutional block attention module. In *ECCV*, 2018. 3
- [22] Wenhan Yang, Robby T. Tan, Jiashi Feng, Jiaying Liu, Zongming Guo, and Shuicheng Yan. Joint rain detection and removal via iterative region dependent multi-task learning. In *CVPR*, 2017. 3
- [23] Rajeev Yasarla, Vishwanath A. Sindagi, and Vishal M. Patel. Syn2real transfer learning for image deraining using gaussian processes. In *CVPR*, 2020. 3
- [24] He Zhang and Vishal M. Patel. Density-aware single image de-raining using a multi-stream dense network. In *CVPR*, 2018. 3
- [25] Kaihao Zhang, Wenhan Luo, Yanjiang Yu, Wenqi Ren, Fang Zhao, Changsheng Li, Lin Ma, Wei Liu, and Hongdong Li. Beyond monocular deraining: Parallel stereo deraining network via semantic prior. In *CVPR*, 2021. 3
- [26] Shangchen Zhou, Jiawei Zhang, Wangmeng Zuo, Haozhe Xie, Jinshan Pan, and Jimmy Ren. Davanet: Stereo deblurring with view aggregation. In *CVPR*, 2019. 3
- [27] Wei Zhou, Ling Zhang, Shengyu Gao, and Xin Lou. Gradient-based feature extraction from raw bayer pattern images. *IEEE Transactions on Image Processing*, 2020. 2
- [28] Wei Zhou, Xiangyu Zhang, Hongyu Wang, Shenghua Gao, and Xin Lou. Raw bayer pattern image synthesis for computer vision-oriented image signal processing pipeline design. *arXiv preprint arXiv:2110.12823*, 2021. 2

## Acknowledgments

We thank Visionary.ai for their joint work and collaboration on this paper.